# Supplementary Information: Generic character of charge and spin density waves in superconducting cuprates

## I. LATTICE PARAMETERS

Table S1 shows lattice parameters of the $La_{1.8-x}Eu_{0.2}Sr_xCuO_4$ (LESCO) samples with $x = 0.07$, 0.10, 0.125, 0.15, 0.17, and 0.20 with a tetragonal unit cell ($a = b$, $\alpha = \beta = \gamma = 90°$). The lattice parameters are determined from single crystal x-ray diffraction measurements with Cu $K_\alpha$ x-ray source.

TABLE S1. Lattice parameters of LESCO with $0.07 \leq x \leq 0.20$.

| $x$ | a (Å) | c (Å) |
|---|---|---|
| 0.07 | 3.806(2) | 13.139(1) |
| 0.10 | 3.79(1) | 13.137(3) |
| 0.125 | 3.79(1) | 13.136(4) |
| 0.15 | 3.79(1) | 13.161(5) |
| 0.17 | 3.79(1) | 13.166(4) |
| 0.20 | 3.77(1) | 13.181(3) |

## II. MEASUREMENT OF HOLE DOPING $p$

Hole doping levels of the LESCO samples are mainly determined by two factors: Sr concentration and oxygen non-stoichiometry. In order to confirm that the doping is controlled by Sr concentration and the effect of oxygen non-stoichiometry is minimal, we have performed x-ray absortpion spectroscopy (XAS) experiments as a direct measurement of hole concentration of the samples. It has been observed that O K edge XAS spectra of hole-doped high-$T_c$ cuprates exhibit two pre-edge peaks and the intensity of the lower energy peak increases linearly with hole concentration in the doping range of 0 to 20% [1–4]. Figure S1(a) shows the O K edge XAS spectra of the LESCO samples that were used in this study, which resemble the spectra of $La_{2-x}Sr_xCuO_4$ reported in Ref. [1]. The pre-edge regions of the result are analyzed in the same way described in Ref. [1], where the background is modeled with a Gaussian function and the two pre-edge peaks (the lower-energy peak: peak A, the higher-energy peak: peak B) are fitted with two Gaussian lineshapes, and the integrated intensities of peak A and B are obtained [Fig. S1(b)]. According to Ref. [1], the relationship between the ratio of the intensities of two pre-edge peaks, $I_{\mathrm{peakA}}/I_{\mathrm{peakB}}$ and the hole doping $p$ is found to be $I_{\mathrm{peakA}}/I_{\mathrm{peakB}} = (11.6 \pm 0.4)p - (0.076 \pm 0.03)$. Using this relationship, we estimated the doping level $p$ of the LESCO samples [Fig. S1(c)] and it agrees well with Sr concentration $x$.

## III. SDW $H$-SCAN AND ONSET TEMPERATURE

Figure S2 shows the $H$-scan of SDW in LESCO $x = 0.125$, where the satellite SDW peaks are present on both side of (0.5, 0.5, 0). The SDW peaks were seen in equivalent points in other Brillouin zones, too. In Fig. S3, the temperature dependence of the integrated intensity of SDW is presented for $x = 0.07$, 0.10, 0.11, and 0.15. The integrated intensities are fitted with the square-root model described in the main manuscript to infer the onset temperatures. The data for $x = 0.125$ is presented in the main manuscript.

## IV. RSXS BACKGROUND SUBTRACTION

Fluorescence background subtraction of RSXS measurements is performed utilizing a large area CCD detector that measures both CDW and fluorescence signals simultaneously, which greatly enhanced the detection sensitivity [5]. The subtraction is done in two steps. As shown in Fig. S4(a), the center part of the CCD images (the region within blue dashed lines) captures the CDW peak profile, while the top and bottom parts (the regions with in orange dashed lines) are far away from the CDW peak and essentially capturing the $H$ dependence of fluorescence intensity. Figure S4(b) shows the raw $H$-scan of CDW (blue curve) and the fluorescence background (orange curve) obtained by averaging

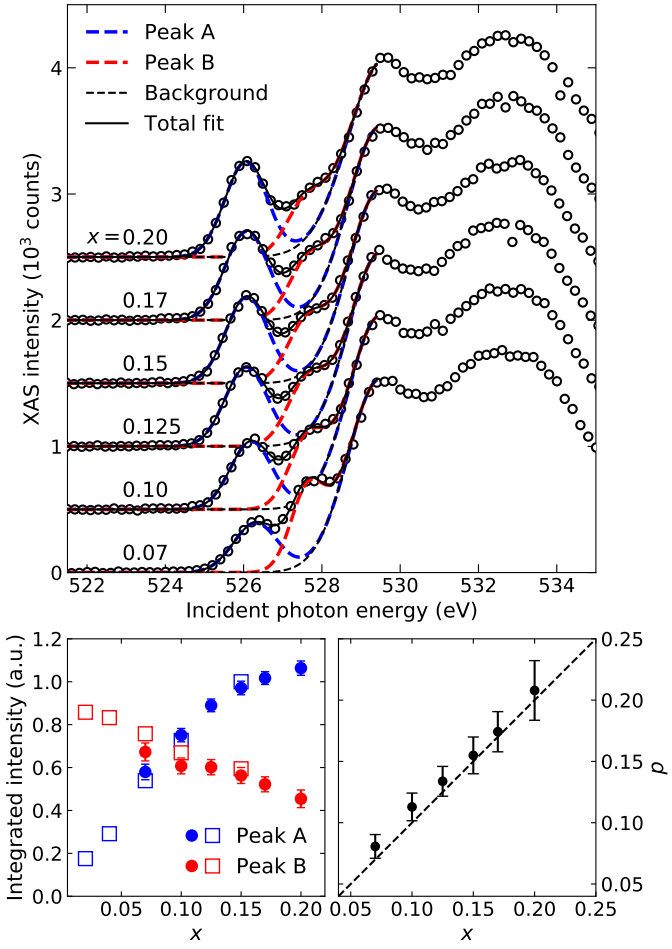


FIG. S1. (a) Oxygen K-edge XAS spectra of LESCO samples. The pre-edge regions of the spectra exhibit two distinct peaks which are fitted with two Gaussian functions (peak A: blue dashed curves, peak B: red dashed curves) and a background (gray dashed curves). The total lineshapes (solid lines) fit well to the XAS data points. (b) Doping evolution of integrated intensities of peak A and B (filled circles). For a comparison, data points from the same analysis on LSCO in Ref. [1] are plotted together (hollow squares). (c) Measured hole doping $p$ plotted against Sr concentration $x$. Dashed line represents $p = x$.

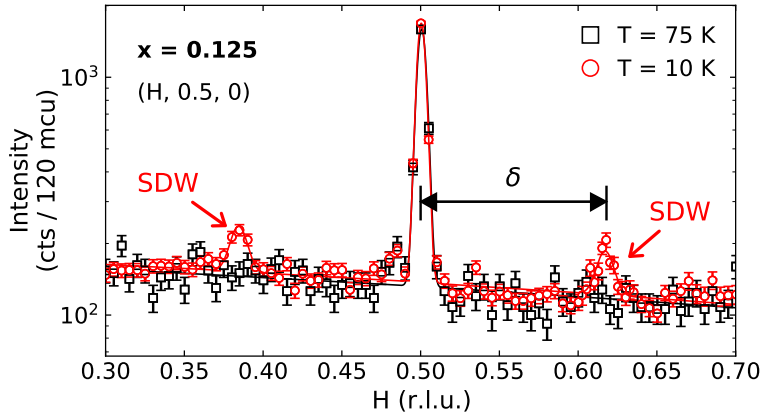


FIG. S2. $H$-scans of SDW of LESCO $x = 0.125$ at temperatures 10 K and 75 K. The SDW peaks are the satellite peaks. The (0.5, 0.5, 0) peak we attribute to multiple scattering. the solid lines are fits to Gaussian functions.

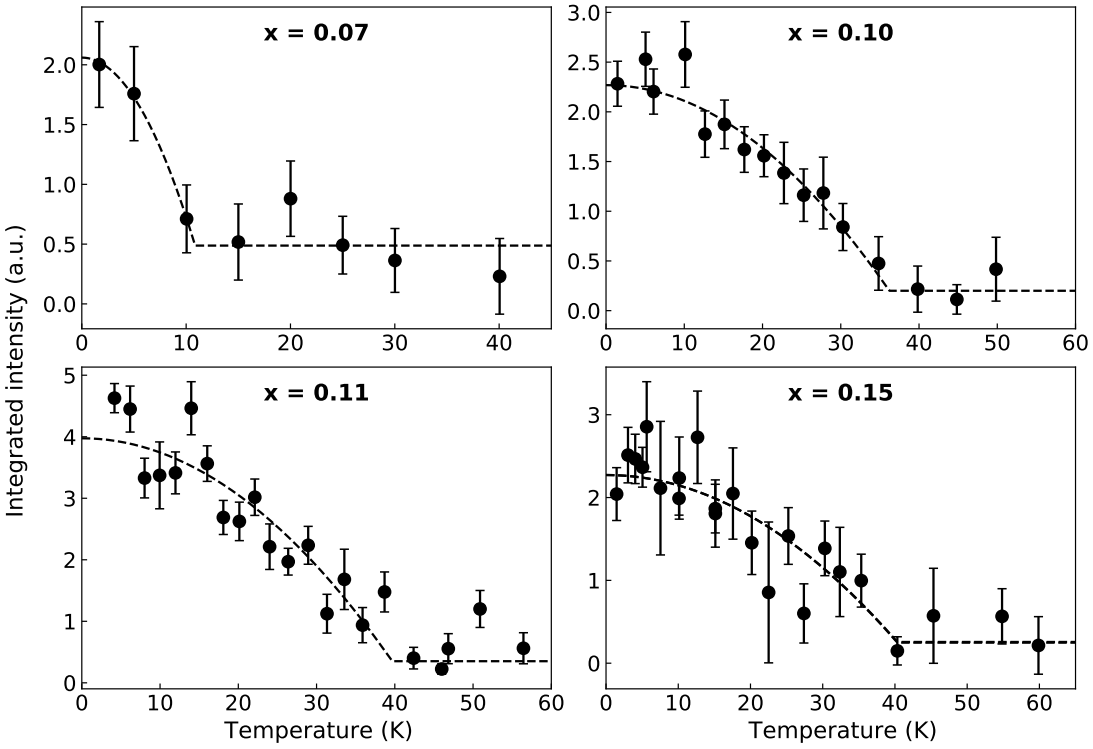


FIG. S3. Integrated intensity of SDW of LESCO $x = 0.07$, 0.10, 0.11, and 0.15. The dashed line shows a fit to Eq. [1] in the main manuscript. Error bars correspond to standard errors.

intensities within each region of the images, and the first background subtraction is carried out by subtracting the two curves. In Fig. S4(c), the result of the first background subtraction (green curve) is plotted, which shows a residual background due to the vertical variation of fluorescence in the CCD images. The remaining background is modeled with a quadratic function (red dashed line) and used for the second background subtraction. The final result after the first and second background subtraction is modeled with a Lorentzian function (brown curve) which fits well to the data.

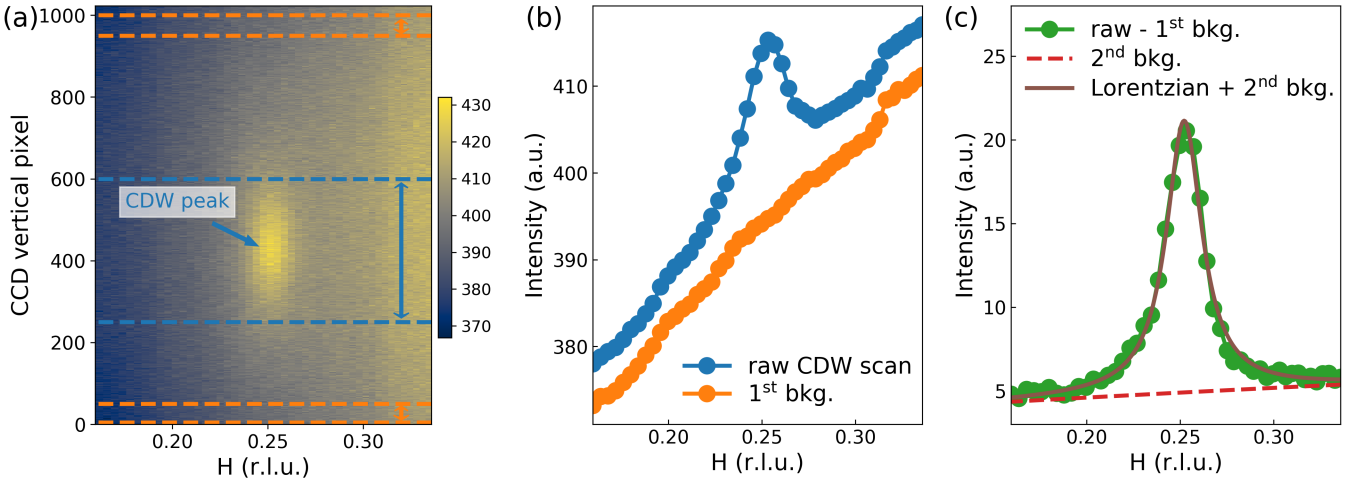


FIG. S4. (a) Intensity map of $H$-scan of CDW of LESCO $x$=0.15 at $T = 23$ K measured using a CCD detector. The region within the blue (orange) dashed lines captures CDW (fluorescence) signals. (b) Raw CDW $H$-scan and the first background curve obtained from the blue and orange region, respectively, in (a). (c) The result of the first background subtraction (green curve) that is fitted with the second background modeled with a quadratic function (red dashed line) and a Lorentzian function (brown curve).

## V. LORENTZIAN FITS AND $S(q,T)$ FITS TO RSXS SCANS

Figure S5 shows the $H$-scans of CDW after background subtraction and Lorentzian fits from which we obtained the peak intensity, correlation length, and wave vector of CDW at each temperature and doping. Figure S6 shows the fitting result with $S(q,T)$ given in Eq. (1) in the main manuscript. The quality of the fit is very good, indicating that the model describes the entire two-dimensional set of $H$-scans (as a function of $q$ and $T$) very well using a single set of temperature-independent parameters.

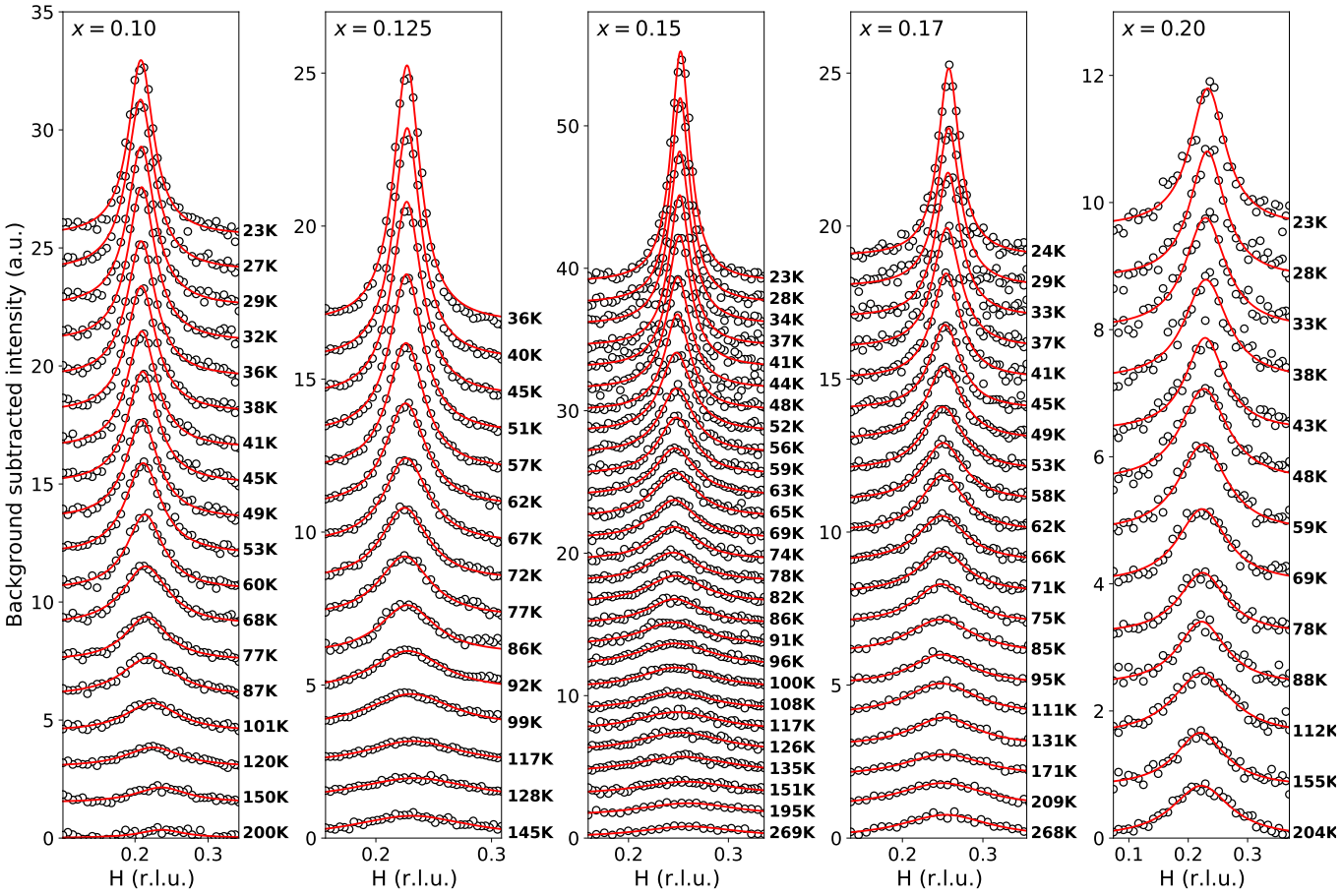


FIG. S5. Background subtracted $H$-scans of CDW of LESCO $x$=0.10, 0.125, 0.15, 0.17 and 0.20 at a wide range of temperature. The solid lines are Lorentzian fits.

## VI. COMPARISON TO A RIXS RESULT

In order to cross-check the results of this study, the temperature dependence of CDW peak intensity and $Q_{\mathrm{CDW}}$ are compared with a previously reported result. Figure S7 shows a comparison with the data from Ref. [6] where a high-resolution ($\Delta E \geq 19$ meV) resonant inelastic x-ray scattering measurement on LESCO $x$=0.125 is reported. The data from this study and Ref. [6] agrees well with each other. Especially, both results exhibit a gradual increase of CDW peak intensity and a kink at $T \sim 75$ K in the temperature evolution of $Q_{\mathrm{CDW}}$.

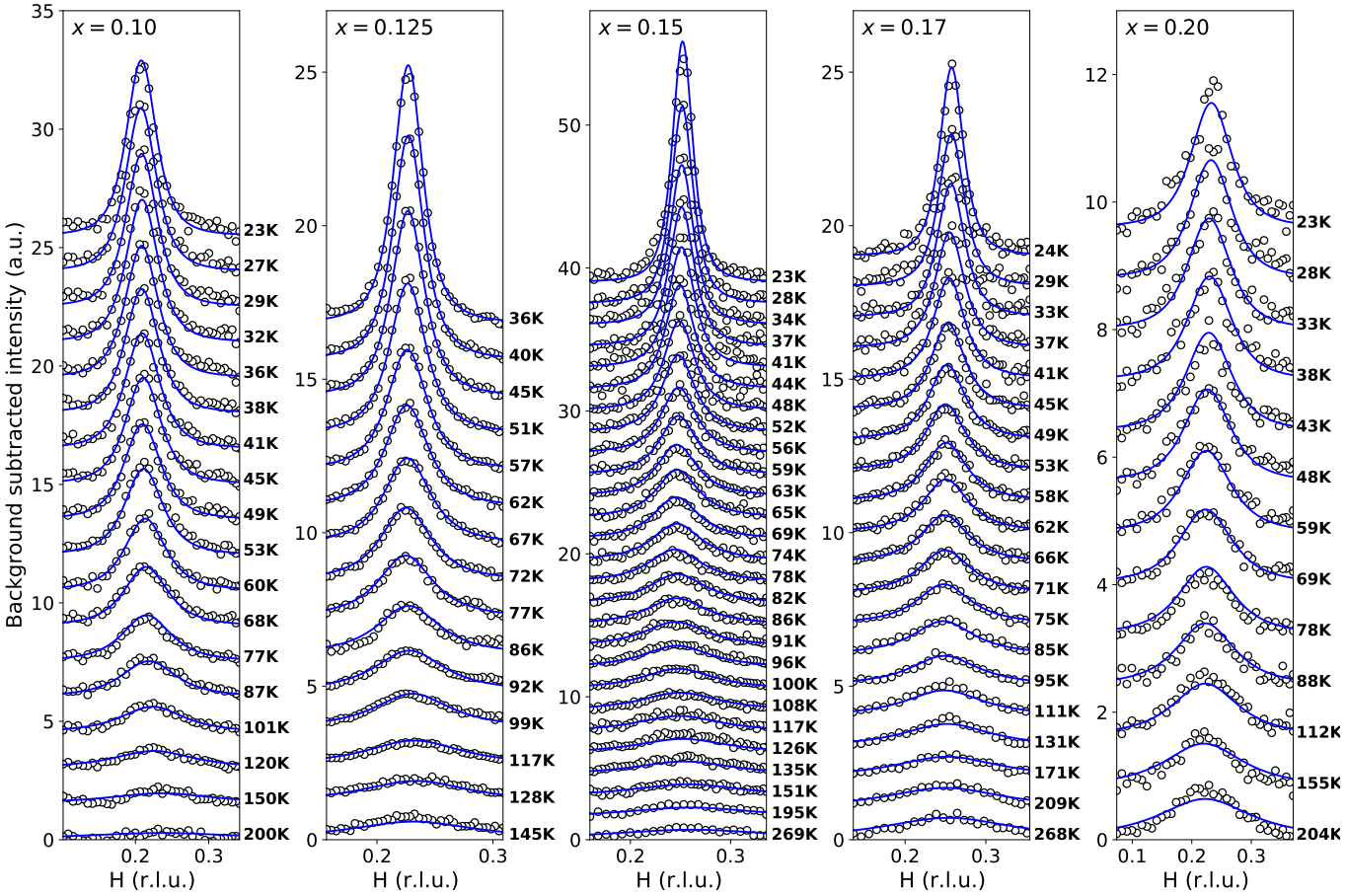


FIG. S6. Background subtracted $H$-scans of CDW of LESCO $x$=0.10, 0.125, 0.15, 0.17 and 0.20 at a wide range of temperature. The solid lines are fits to $S(q,T)$ given in Eq (1) in the main manuscript.

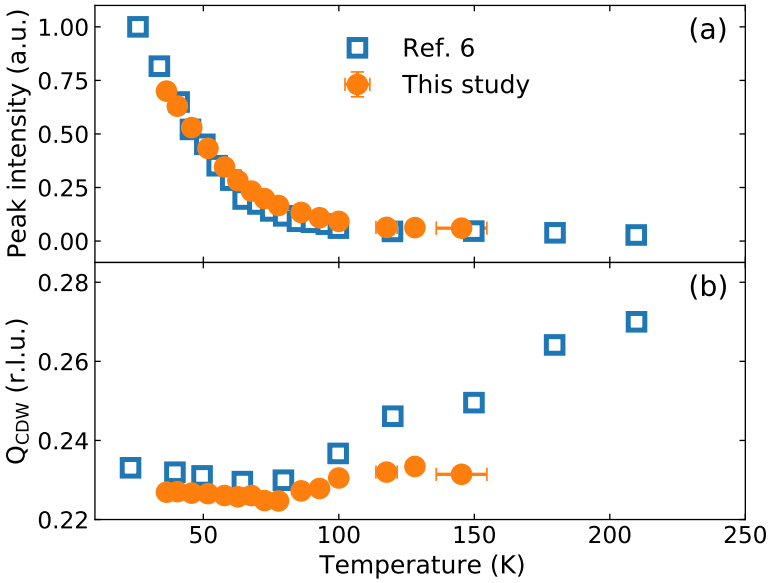


FIG. S7. Comparison of temperature dependence of (a) CDW peak intensity and (b) $Q_{\mathrm{CDW}}$ in LESCO $x$=0.125 reported in Ref. [6] (hollow squares) and measured in this study (filled circles).

## VII. SUPPLEMENTARY THEORY MATERIAL

### A. Summary of experimental facts

The experimental results from x-ray diffraction and neutron scattering are summarized as follows:

1. X-ray diffraction studies of Eu-doped $La_{2-x}Sr_xCuO_4$ (LESCO) samples with doping in the range $0.1 < x < 0.2$ and temperatures in the range $15K < T < 250K$ show CDW order.

2. The CDW ordering wave vector $\boldsymbol{Q}_{\rm CDW} = Q_{\rm CDW}\hat{\boldsymbol{a}}$ and varies with doping and with temperature. Here $\hat{\boldsymbol{a}}$ is a unit vector along the $a$ direction of the Cu-O plane. We assume that the CDW order is unidirectional, in line with previous experimental findings in cuprates [7, 8].

3. The onset of CDW order is broad, and essentially the same for all dopings. The CDW order it is well developed well above the structural transition and it is essentially unaffected by it.

4. For much of the measured temperature range the integrated intensity of the CDW peak is essentially temperature-independent, indicating that the strength of the CDW order parameter (i.e. its amplitude) is essentially constant in the measured range of temperatures (although it is different at different doping levels).

5. Neutron scattering data shows that these samples exhibit SDW order below a temperature which depends on doping.

6. The SDW transition is fairly broad, and the SDW incommensuration $\delta$ appears to be temperature-independent and doping-dependent. We, again, assume the order is unidirectional.

7. Except for the very underdoped sample (with $x \sim 0.1$) the temperature dependence of the CDW ordering wave vector $Q_{\rm CDW}$ is not monotonic, decreasing with lowering temperatures down to minimum below which it increases rapidly.

8. The kink in the $T$ dependence of $Q_{\rm CDW}$ appears to occur near the experimental onset temperature of SDW obtained from the neutron scattering results.

9. At low temperatures the (incommensurate) CDW and SDW orders become commensurate with each other and exhibit the characteristic relation $Q_{\rm CDW} = 2\delta$ observed in $La_{2-x}Ba_xCuO_4$ (LBCO) and in $La_{1.6-x}Nd_{0.4}Sr_xCuO_4$ (LNSCO).

Several conclusions emerge from these experimental results. The fact that, for given doping level, the amplitude of the order parameter is essentially independent of the temperature suggests that the thermal fluctuations of the *phase* of the CDW order parameter play a dominant role (at least for some of the phenomena), i.e. a non-linear sigma model approach may give a good description. Also, the fact that the CDW thermal transition is broad implies that disorder plays a key role as a "random field" effect coupled linearly to the CDW order parameter. This approach is presented below. On the other hand, the fact that the CDW ordering wave vector varies significantly with temperature and doping strongly suggests that a finite electronic compressibility must be part of the explanation of the observed phenomena. This effect is not easily accounted for in a simple non-linear sigma model approach. Similarly, the theory must also describe the mutual commensurability of the CDW and the SDW orders, which is more easily described in a landau-Ginzburg approach, as is the temperature dependence of $Q_{\rm CDW}$. For the sake of simplicity we will use both approaches.

### B. Landau-Ginzburg Theory

#### *1. CDW alone*

We will consider first the case when there is only CDW order. The Landau-Ginzburg theory for a CDW in a system with finite charge compressibility was discussed in Ref. [9], which is an extension of the standard Landau theory for CDW due to McMillan [10] for a system with finite compressibility. We will consider a 3D system with unidirectional order, with ordering wave vector $\boldsymbol{Q} = Q\hat{\boldsymbol{Q}}$. Here follow closely Ref.[9].

In a CDW phase the local charge density has the expansion

$$\rho(\boldsymbol{x}) = \psi_0(\boldsymbol{x}) + i\Lambda\psi^*(\boldsymbol{x})\hat{\boldsymbol{Q}}\cdot\boldsymbol{\nabla}\psi(\boldsymbol{x}) + \text{c.c.} + \psi(\boldsymbol{x})\exp(i\boldsymbol{Q}\cdot\boldsymbol{x}) + \psi^*(\boldsymbol{x})\exp(-i\boldsymbol{Q}\cdot\boldsymbol{x}) + \ldots \quad (1)$$

The complex field $\psi(\boldsymbol{x})$ is the order parameter of the CDW and we have kept only the leading harmonic. The real field $\psi_0(\boldsymbol{x})$ represents the long wavelength fluctuations of the charge density and represents the finite charge compressibility. The second term in Eq.(1) is McMillan's "CDW compression term" and describes the contribution of the local fluctuations of the CDW order parameter to the long wavelength charge fluctuations. Finally, $\boldsymbol{Q}$ is the "ideal" CDW ordering wave vector.

We will see below that the finite compressibility leads to temperature-dependent deviations of the actual ordering wave vector from the ideal value (McMillan's theory this effect is introduced "by hand"). The average charge density is given by $L^3\bar{\rho} = \int d^3x \rho(\boldsymbol{x})$. We will assume that the charge density has a preferred "normal" density $\rho_N$. The difference $\Delta\bar{\rho} = \bar{\rho} - \rho_N$ will play the role of a control parameter and, qualitatively, can be thought of as representing the doping level.

The CDW Landau-Ginzburg free energy is

$$F_{\rm CDW} = \int d^3x \Big\{ \frac{1}{2} K_c \Big| \Big( i\hat{\boldsymbol{Q}} \cdot \boldsymbol{\nabla} + \delta_0 \Big) \psi(\boldsymbol{x}) \Big|^2 + \frac{r_c}{2} |\psi(\boldsymbol{x})|^2 + u_c |\psi(\boldsymbol{x})|^4 \Big\} + \int d^3x \frac{\kappa_0}{2} (\psi_0(\boldsymbol{x}) - \rho_N)^2 + \frac{1}{2} \int d^3x \int d^3y (\rho(\boldsymbol{x}) - \bar{\rho}) V(|\boldsymbol{x} - \boldsymbol{y}|) (\rho(\boldsymbol{y}) - \bar{\rho}) \tag{2}$$

Here $K_c$ is the stiffness of the CDW order parameter, $\delta_0$ is the "pressure", $r_c = T - T^0_{\rm CDW}$ (with $T^0_{\rm CDW}$ being the usual mean field CDW critical temperature), and $u_c$ are the usual parameters of the Landau potential.

In the free energy of Eq.(2) $\kappa_0$ is the uniform charge compressibility and plays an important role in the physics: for $\kappa_0 \to \infty$ there is no screening and for $\kappa_0 \to 0$ the interaction becomes ultra-local. The last term represents the long-range Coulomb interaction of the charge configurations $\rho(\boldsymbol{x})$ given in Eq.(1), and

$$V(|\boldsymbol{x} - \boldsymbol{y}|) = \frac{e^2}{\varepsilon} \frac{1}{|\boldsymbol{x} - \boldsymbol{y}|} \tag{3}$$

where $\varepsilon$ is the dielectric constant.

The equilibrium state is obtained by the extrema of the free energy of Eq.(2) with respect to the uniform component $\psi_0$ and with respect to the CDW order parameter $\psi$. Among other things, the fluctuations of the uniform component lead to the screening of the long-range Coulomb interaction, with a screening length $\xi = \left( \frac{4\pi\varepsilon}{e^2} \kappa_0 \right)^{1/2}$ tuned by the compressibility $\kappa_0$. Thus, if $\kappa_0 \to \infty$ there is no screening and if $\kappa_0 \to 0$ the interaction is ultra-local.

We will look for the extrema of the LG free energy with an ICDW ansatz $\psi(x) = \phi_0 \exp(i\hat{\boldsymbol{Q}} \cdot \boldsymbol{x}\delta)$, where $\delta$ is the incommensuration and $\phi_0$ is the CDW amplitude. Hence, the actual CDW ordering wave vector has a magnitude $Q_{\rm CDW} = Q + \delta$, along the direction $\hat{\boldsymbol{Q}}$.

We will need to determine also the average value of the compressible charge density $\bar{\psi}_0$. In this state $\bar{\psi}_0$ is given by

$$\bar{\psi}_0 = \bar{\rho} - 2\Lambda |\phi_0|^2 \delta \tag{4}$$

which shows that the incommensuration $\delta$ shifts the average value of the compressible charge density away from the average density $\bar{\rho}$.

In the normal state $\psi = 0$, $\rho(\boldsymbol{x}) = \bar{\rho} = \bar{\psi}_0$. The free energy in the normal state is $F_N = \frac{1}{2} L^3 \kappa_0 (\Delta\bar{\rho})^2$.

The free energy density in the CDW state becomes

$$f_{\rm CDW} = \frac{1}{2} K_c (\delta - \delta_0)^2 |\phi_0|^2 + \frac{1}{2} \left( r_c + 2\tilde{V}_{\rm eff}(Q_{\rm CDW}) \right) |\phi_0|^2 + u_c |\phi_0|^4 + \frac{\kappa_0}{2} (\Delta\bar{\rho} + 2\Lambda |\phi_0|^2 \delta)^2 \tag{5}$$

where

$$\tilde{V}_{\rm eff}(Q_{\rm CDW}) = \frac{\frac{e^2}{4\pi\varepsilon}}{Q^2_{\rm CDW} + \xi^{-2}} \tag{6}$$

is the Fourier transform of the screen Coulomb interaction at the wave vector $Q_{\rm CDW}$ and $\xi$ is the screening length.

Upon extremizing with respect to $\delta$ the free energy density in the ICDW state, Eq.(5), we obtain

$$\delta = \delta_0 \left( \frac{b^2 - a^2}{b^2 + |\phi_0|^2} \right) \tag{7}$$

where we defined

$$a^2 = \frac{\Delta\bar{\rho}}{2\Lambda\delta_0}, \qquad b^2 = \frac{K_c}{4\Lambda^2 \kappa_0} \tag{8}$$

Eq.(7) shows that the incommensuration $\delta$ depends explicitly on $\phi_0$, the amplitude of the CDW, which depends on the temperature. Thus, as the amplitude of the CDW order parameter $\phi_0$ increases (with decreasing temperature), the value of the incommensuration $\delta$ will decrease (increase) for $b > a$ (for $b < a$). Notice that in the ultra-local limit, where $\kappa_0 \to 0$, $\delta \to \delta_0$ and has no temperature dependence.

By plugging in the expression for $\delta$ of Eq.(7) back into of Eq.(5), we obtain the expression for the free energy density [9],

$$f_{\rm CDW} = \frac{1}{2}K_c\delta_0^2\,\frac{(a^2+|\phi_0|^2)^2}{b^2+|\phi_0|^2} + \frac{1}{2}(r_c + 2\tilde{V}_{\rm eff}(Q_{\rm CDW}))|\phi_0|^2 + u_c|\phi_0|^4 \tag{9}$$

This expression differs from the conventional expression for the CDW free energy density in two respects. A minor one is the shift of the coefficient $r_c = T - T^0_{\rm CDW}$ by the Coulomb potential at the CDW wave vector. This shift means that the naive CDW critical temperature is suppressed by the Coulomb effect. However, in addition we now have the much more non-linear first term which plays a key role. The origin of this term is the finite compressibility. In fact, as $\kappa_0$ increases, where screening becomes poorer, this term shifts the critical temperature of the CDW to high temperature.

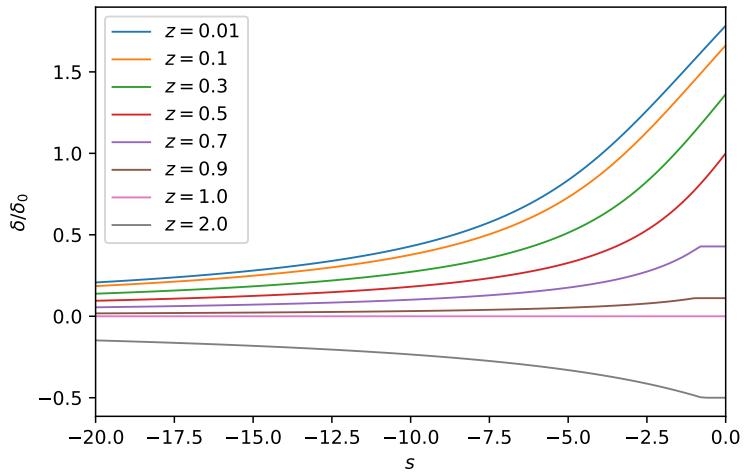


FIG. S8. Incommensurability $\delta$ as a function of temperature (represented by $s$) for different values of $z$, controlled by the compressibility $\kappa_0$.

A numerical minimization of the CDW free energy density, Eq.(9), yields a plot of the CDW amplitude $\phi_0$ and of the incommensurability $\delta$ as a function of temperature (shown in Fig.S8). In the figure a plot of the data for the discommensuration $\frac{\delta}{\delta_0}$, Eq.(7) is shown parametrized by the dimensionless quantities $z = \frac{b^2}{a^2}$ (with $a$ and $b$ defined in Eq.(8)) and $x = \frac{|\phi_0|^2}{b^2}$, and $s = (r_c + 2\tilde{V}_{\rm eff}(Q_{\rm CDW})/K_c\delta_0^2$.

The upshot of these results is that a monotonic temperature-dependence of the CDW ordering wave vector can be explained as a consequence of the finite compressibility. In addition, the extrapolated value of the ordering wave vector at the nominal onset of CDW order can be related to the doping level, qualitatively represented by $\Delta\bar{\rho}$, and hence by $a^2$. However, these expressions alone cannot describe the non-monotonic behavior seen in the experiments. Next we will see that the non-monotonicity can be explained by the interaction between the CDW and the SDW.

### *2. CDW+SDW*

We now turn to the full problem, including the SDW and its interaction with the CDW. In an SDW state local magnetization $\boldsymbol{M}(\boldsymbol{x})$ has an expansion in harmonics of the ordering wave vector $\boldsymbol{K}$ of the form

$$\boldsymbol{M}(\boldsymbol{x}) = \boldsymbol{S}(\boldsymbol{x})\exp(i\boldsymbol{K}\cdot\boldsymbol{x}) + \text{c.c.} \tag{10}$$

where we kept only the leading harmonic. The SDW order parameter $\boldsymbol{S}(\boldsymbol{x})$ is a three-component complex field. In its simplest form the free energy of the SDW order parameter is (see Refs. [11] and [12])

$$F_{\rm SDW} = \int d^3x \Big\{ \frac{1}{2} K_s \left| \boldsymbol{\nabla} S_a(\boldsymbol{x}) \right|^2 + \frac{1}{2} r_s |\boldsymbol{S}(\boldsymbol{x})|^2 + u_s |\boldsymbol{S}(\boldsymbol{x})|^4 + \tilde{u}_s |\boldsymbol{S}^*(\boldsymbol{x}) \times \boldsymbol{S}(\boldsymbol{x})|^2 \Big\} \tag{11}$$

(with $a = 1, 2, 3$) where $r_s = T - T_0^{\rm SDW}$ and $u_s > 0$. We will be interested only in collinear spin order and we will set $\tilde{u}_s = 0$.

The free energy of the full system, involving both charge and spin orders, is

$$F = F_{\rm CDW} + F_{\rm SDW} + F_{\rm int} \tag{12}$$

where $F_{\rm CDW}$ is given in Eq.(2) and $F_{\rm SDW}$ in Eq.(11). The third term in Eq.(12) is

$$F_{\rm int} = \int d^3x \Big\{ \lambda \psi^*(\boldsymbol{x}) \boldsymbol{S}(\boldsymbol{x}) \cdot \boldsymbol{S}(\boldsymbol{x}) \exp(i(2\boldsymbol{K} - \boldsymbol{Q}) \cdot \boldsymbol{x}) + \text{c.c.} + \gamma |\psi(\boldsymbol{x})|^2 |\boldsymbol{S}(\boldsymbol{x})|^2 \Big\} \tag{13}$$

Here, $\lambda$ and $\gamma$ are two coupling constants. The important coupling is $\lambda$ which describes the effects of mutual commensurability of the CDW and SDW orders. We will only consider the case in which the SDW onsets at temperatures well below the CDW, and so we will take $T_{\rm SDW}^0 \ll T_{\rm CDW}^0$, which is the experimentally relevant situation in LESCO. Thus, the CDW order is well developed at the temperature for the onset of the SDW.

It is convenient to parametrize the magnitudes of the ordering wave vectors of the coupled CDW and SDW as follows

$$Q_{\rm CDW} = Q + 2\ell, \qquad K_{\rm SDW} = K + \ell - q \tag{14}$$

where we used the notation $\delta = 2\ell$. Here $q$ measures the mutual incommensurability of the CDW and the SDW.

The mean field ansatz now is

$$\psi(\boldsymbol{x}) = \phi_0 \exp(i 2\ell\, \hat{\boldsymbol{Q}} \cdot \boldsymbol{x}), \qquad \boldsymbol{S}(\boldsymbol{x}) = \boldsymbol{S}_0 \exp(i(\ell - q) \hat{\boldsymbol{Q}} \cdot \boldsymbol{x}) \tag{15}$$

where, for the case of interest, $\phi_0$ and $\boldsymbol{S}_0$ can be chosen to be a real amplitude and a real vector, respectively. The full free energy density for this ansatz is

$$\begin{aligned} f =& f_{\rm CDW} + f_{\rm SDW} + f_{\rm int} \\ =& \frac{1}{2} K_c (2\ell - \delta_0)^2 \phi_0^2 + \frac{1}{2} \left( r_c + 2\tilde{V}_{\rm eff}(Q_{\rm CDW}) \right) \phi_0^2 + u_c \phi_0^4 + \frac{\kappa_0}{2} (\Delta\bar{\rho} + 2\Lambda |\phi_0|^2 \delta)^2 \\ &+ \frac{1}{2} (r_s + K_s (\ell - q)^2)\ \boldsymbol{S}_0^2 + u_s\ \boldsymbol{S}_0^4 + 2\lambda \phi_0 \boldsymbol{S}_0^2 + \gamma \phi_0^2 \boldsymbol{S}_0^2 \end{aligned} \tag{16}$$

where the second line is the same as Eq.(9) (with $\delta = 2\ell$).

It is convenient to introduce the parametrization

$$x = \frac{\phi_0}{a}, \qquad y = \frac{S_0}{c}, \qquad t = \frac{q}{\delta_0}, \qquad a^2 = \frac{\Delta\bar{\rho}}{2\Lambda\delta_0}, \qquad b^2 = \frac{K_c}{4\Lambda^2\kappa_0}, \qquad z = \frac{b^2}{a^2}, \qquad c^2 = \frac{16\Lambda^2\kappa_0}{K_s} a^4 \tag{17}$$

Extremizing the free energy of Eq.(16) with respect to $\ell$ we now find

$$\ell = \frac{\delta_0}{2} \Big[ \frac{x^2(z-1) + 2ty^2}{x^2(z + x^2) + y^2} \Big] \tag{18}$$

The equilibrium state is now found by finding the minimum of the free energy with respect to $\phi_0$ and $S_0$. In terms of the parametrization defined in Eq.(17) and the expression for $\ell$ of Eq.(18), the free energy density of Eq.(16) takes the form

$$f = \frac{1}{2} K_c \delta_0^2 a^2 F(x, y) \tag{19}$$

where

$$\begin{aligned} F(x,y) =& \Big[ \frac{x^2(x^2+1) - (2t-1)y^2}{x^2(x^2+z) + y^2} \Big]^2 x^2 + \frac{x^2}{z} \Big[ \frac{z(x^2+1) + 2ty^2}{x^2(x^2+z) + y^2} \Big]^2 + \mu y^2 \Big[ \frac{x^2(z - 1 - 2t(x^2+z)}{x^2(x^2+z) + y^2} \Big]^2 \\ &+ \tilde{r}_c x^2 + w_c x^4 + \tilde{r}_s y^2 + w_s y^4 + \tilde{\gamma} x^2 y^2 + \tilde{\lambda} x y^2 \end{aligned} \tag{20}$$

Here we used the rescaled parameters

$$\tilde{r}_c = \frac{(r_c + 2\tilde{V}(Q)}{K_c\delta_0^2}, \qquad w_c = \frac{2a^2}{K_c\delta_0^2}u_c, \qquad \tilde{r}_s = \frac{c^2}{K_c a^2\delta_0^2}r_s, \qquad w_s = \frac{2c^4}{K_c\delta_0^2 a}u_s$$
$$\tilde{\gamma} = \frac{2c^2}{K_c\delta_0^2}\gamma, \qquad \tilde{\lambda} = \frac{4c^2}{K_c\delta_0^2 a}\lambda, \qquad \mu = \frac{1}{z} \tag{21}$$

The resulting equilibrium state exhibits the expected non-monotonic behavior of the ordering wave vectors as a function of temperature, showing a kink as the CDW and SDW orders begin to converge to a state close to mutually commensurability (controlled by $q$). An example is shown in Fig.S9.

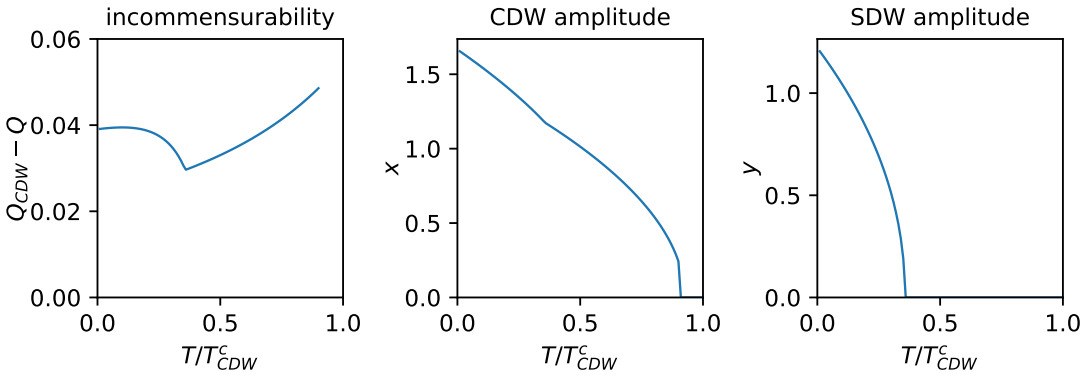


FIG. S9. Incommensurability $\ell$, CDW order parameter $x$ and SDW order parameter $y$ as a function of temperature for typical values of the parameters of the free energy of Eq.(20).

### *3. Incommensurability fitting*

The temperature dependence of the incommensurability, as plotted in Fig. {main text figure}, can be fit to the model by considering the parameters in Eq. (21), minimizing Eq. (20) with respect to the rescaled order parameters $x$ and $y$, and determining the ordering wavevectors via Eq. (14) and Eq. (18). Temperature dependence is contained implicitly in the parameters

$$\tilde{r}_c = a_c(T - T^c_{\rm CDW}), \qquad \tilde{r}_s = a_s(T - T^c_{\rm SDW}). \tag{22}$$

Here we have introduced the parameters $a_c$ and $a_c$, to convert $\tilde{r}_c$ and $\tilde{r}_s$ into Kelvin. $T^c_{\rm CDW}$ and $T^c_{\rm SDW}$ represent nominal ordering temperatures of CDW and SDW, respectively, i.e. the ordering temperatures in the absence of compressibility effects and coupling between CDW and SDW. The actual ordering temperatures, determined by minimizing Eq. (20), can vary slightly for the CDW transition and moderately for the SDW transition.

To reduce the number of parameters involved, we fix a few parameters as follows. Noting that the experimental data does not show a clear transition up to $\sim 300$K, we interpret the charge ordering as having a very high mean-field transition temperature and hence fix $T^c_{\rm CDW} = 400$K. For the nominal SDW ordering temperature, we fix $T^c_{\rm SDW} = 35$K to be roughly consistent with the SDW onset temperature seen in neutron scattering. Finally, the effect of the coupling $\tilde{\gamma}$ can be mimicked by varying the magnitude of $\tilde{\lambda}$. Therefore, $\tilde{\gamma}$ is not strongly constrained and we set it to 0 for simplicity; the quality of the final fits is not affected.

The remaining parameters $Q, \delta_0, \tilde{\lambda}, z, t, a_c, a_s$ are free. We numerically optimize over the space of these parameters, minimizing $F(x, y)$ and calculating $Q_{\rm CDW}$ as a function of $T$ for each parameter set, to obtain a least-squares fit to the experimental data of incommensurability. The obtained parameters are shown in Table. S2. In all cases, the fit is successful, with the statistic $\chi^2 \sim N$, where $N$ is the number of experimental data points.

## C. Disorder and the Non-linear Sigma Model

We have not included the effects of quenched disorder in the free energy of Eq.(2). The local electrostatic potential $V_{\rm dis}(\boldsymbol{x})$ generated by quenched disorder couples linearly to the local charge density through a term of the form

| $x$ | $Q$ | $\delta_0$ | $\tilde{\lambda}$ | $z$ | $t$ | $a_c$ | $a_s$ |
|---|---|---|---|---|---|---|---|
| 0.10 | 0.0561 | 0.387 | -0.122 | 2.96 | 0.572 | 0.0247 | 0.018 |
| 0.125 | 0.106 | 0.293 | -0.899 | 2.65 | 0.523 | 0.0198 | 0.0283 |
| 0.15 | 0.132 | 0.197 | -1.32 | 4.1 | 1.23 | 0.0178 | 0.0202 |
| 0.17 | 0.246 | 0.114 | -3.58 | 1.08 | 1.16 | 0.0213 | 0.00429 |
| 0.20 | 0.23 | 0.0522 | -0.946 | 0.775 | 0.373 | 0.0151 | 0.0562 |

TABLE S2. Landau-Ginzburg fitting parameters.

$F_{\text{disorder}} = \int d^3x V_{\text{dis}}(\boldsymbol{x})\rho(\boldsymbol{x})$. Thus, disorder acts a local "random field" coupled linearly to the CDW order parameter $\psi(\boldsymbol{x})$. As it is well known [13], below a critical dimension quenched disorder destroys long range order. In systems with continuous symmetries, such as an ICDW, it completely destroys the true long range order below four dimensions.

For a basic characterization of the effects of disorder on the structure factor. This problem was discussed extensively in the literature of the Ising model in random fields and related systems [14–16]. Here we follow the more recent discussion of Ref. [17] and write the structure factor $S$ in terms of an ideal disorder-free susceptibility $G$

$$S(Q_{\text{CDW}} + q) = TG(q) + \sigma^2 G^2(q) \tag{23}$$

$$G(q) = \frac{1}{\kappa_\parallel q_x^2 + \kappa_\perp q_y^2 + \mu}. \tag{24}$$

Here, $\sigma$ characterizes the disorder strength, $\kappa_\parallel$ and $\kappa_\perp$ are coefficients of gradient terms in the effective Hamiltonian of [17]. The peak width is determined by the ratio of $\mu$ to $\kappa_\parallel$. The temperature dependence is contained implicitly in $\mu$. After approximating the system as a non-linear sigma model, $\mu$ can be determined self-consistently by the condition

$$1 = \int \frac{d^2q}{(2\pi)^2} S(q). \tag{25}$$

Inserting Eq. (23) gives

$$1 = TA_1(\mu) + \sigma^2 A_2(\mu) \tag{26}$$

where

$$A_n(\mu) = \int \frac{d^2q}{(2\pi)^2} [G(q)]^n. \tag{27}$$

Evaluating for $n = 1, 2$,

$$A_2(\mu) = \frac{1}{4\pi\sqrt{\kappa_\parallel \kappa_\perp}} \frac{1}{\mu} \tag{28}$$

$$A_1(\mu) = \frac{1}{4\pi\sqrt{\kappa_\parallel \kappa_\perp}} \int_\mu^\Gamma \frac{dx}{x} \tag{29}$$

$$= \frac{1}{4\pi\sqrt{\kappa_\parallel \kappa_\perp}} \ln \frac{\Gamma}{\mu} \tag{30}$$

where $\Gamma$ is a UV cutoff. Thus, the temperature dependence of $\mu$ is determined by

$$4\pi\sqrt{\kappa_\parallel \kappa_\perp} = T \ln \left[\frac{\Gamma}{\mu}\right] + \frac{\sigma^2}{\mu}. \tag{31}$$

For simplicity, below we will work with $\kappa_\parallel = \kappa_\perp = \kappa$.

### 1. *$S(Q)$ lineshape fitting*

The parameters $\sigma^2, \kappa, \Gamma$ make a precise prediction for the evolution of the lineshape of $S(Q)$ as a function of temperature. The applicability of this model can be seen by fitting the entirety of momentum and temperature dependence in

the $S(Q,T)$ using Eq. (23) with temperature-independent parameters $\sigma^2, \kappa, \Gamma$ and an overall temperature-independent normalization. (Here, since we are only fitting the lineshape, we always consider momentum relative to $Q_{\rm CDW}$). Despite the simplicity of the model, having only four temperature-indepedent parameters, we find that the entire range of temperature in the experimental data, spanning around an order of magnitude, can be fit surprisingly well. The obtained parameters are shown in Table. S3. This suggests that our highly approximate model provides an appropriate description of the effects of disorder on the lineshape of the spectra and its temperature dependence.

| $x$ | $\sigma$ | $\kappa$ | $\Gamma$ | $A$ |
|---|---|---|---|---|
| 0.10 | 4.28 | 38.4 | 7.49 | $9.65\times10^{-4}$ |
| 0.125 | 1.56 | 28.1 | 1.42 | $5.13\times10^{-4}$ |
| 0.15 | 1.10 | 22.3 | 0.663 | $6.08\times10^{-4}$ |
| 0.17 | 1.13 | 16.4 | 0.362 | $4.46\times10^{-4}$ |
| 0.20 | 4.41 | 22.9 | 0.782 | $6.30\times10^{-4}$ |

TABLE S3. $S(Q,T)$ fitting parameters. $A$ is an overall normalization factor.


[1] C. T. Chen, F. Sette, Y. Ma, M. S. Hybertsen, E. B. Stechel, W. M. C. Foulkes, M. Schulter, S.-W. Cheong, A. S. Cooper, L. W. Rupp, B. Batlogg, Y. L. Soo, Z. H. Ming, A. Krol, and Y. H. Kao, Electronic states in $La_{2-x}Sr_xCuO_{4+\delta}$ probed by soft-x-ray absorption, Phys. Rev. Lett. **66**, 104 (1991).

[2] E. Pellegrin, N. Nücker, J. Fink, S. L. Molodtsov, A. Gutiérrez, E. Navas, O. Strebel, Z. Hu, M. Domke, G. Kaindl, S. Uchida, Y. Nakamura, J. Markl, M. Klauda, G. Saemann-Ischenko, A. Krol, J. L. Peng, Z. Y. Li, and R. L. Greene, Orbital character of states at the fermi level in $La_{2-x}Sr_xCuO_4$ and $R_{2-x}Ce_xCuO_4$ (R=Nd,Sm), Phys. Rev. B **47**, 3354 (1993).

[3] D. C. Peets, D. G. Hawthorn, K. M. Shen, Y.-J. Kim, D. S. Ellis, H. Zhang, S. Komiya, Y. Ando, G. A. Sawatzky, R. Liang, D. A. Bonn, and W. N. Hardy, X-ray absorption spectra reveal the inapplicability of the single-band hubbard model to overdoped cuprate superconductors, Phys. Rev. Lett. **103**, 087402 (2009).

[4] C.-C. Chen, M. Sentef, Y. F. Kung, C. J. Jia, R. Thomale, B. Moritz, A. P. Kampf, and T. P. Devereaux, Doping evolution of the oxygen $k$-edge x-ray absorption spectra of cuprate superconductors using a three-orbital hubbard model, Phys. Rev. B **87**, 165144 (2013).

[5] J.-J. Wen, H. Huang, S.-J. Lee, H. Jang, J. Knight, Y. S. Lee, M. Fujita, K. M. Suzuki, S. Asano, S. A. Kivelson, C.-C. Kao, and J.-S. Lee, Observation of two types of charge-density-wave orders in superconducting $La_{2-x}Sr_xCuO_4$, Nature Communications **10**, 3269 (2019).

[6] Q. Wang, M. Horio, K. von Arx, Y. Shen, D. John Mukkattukavil, Y. Sassa, O. Ivashko, C. E. Matt, S. Pyon, T. Takayama, H. Takagi, T. Kurosawa, N. Momono, M. Oda, T. Adachi, S. M. Haidar, Y. Koike, Y. Tseng, W. Zhang, J. Zhao, K. Kummer, M. Garcia-Fernandez, K.-J. Zhou, N. B. Christensen, H. M. Rønnow, T. Schmitt, and J. Chang, High-temperature charge-stripe correlations in $La_{1.675}Eu_{0.2}Sr_{0.125}CuO_4$, Phys. Rev. Lett. **124**, 187002 (2020).

[7] R. Comin, R. Sutarto, E. H. da Silva Neto, L. Chauviere, R. Liang, W. N. Hardy, D. A. Bonn, F. He, G. A. Sawatzky, and A. Damascelli, Broken translational and rotational symmetry via charge stripe order in underdoped yba¡sub¿2¡/sub¿cu¡sub¿3¡/sub¿o¡sub¿6+¡/sub¿¡i¿¡sub¿y¡/sub¿¡i¿, Science **347**, 1335 (2015), https://www.science.org/doi/pdf/10.1126/science.1258399.

[8] R. Comin and A. Damascelli, Resonant x-ray scattering studies of charge order in cuprates, Annual Review of Condensed Matter Physics **7**, 369 (2016).

[9] S. E. Brown, E. Fradkin, and S. A. Kivelson, Surface pinning of fluctuating charge order: An extraordinary surface phase transition, Phys. Rev. B **71**, 224512 (2005).

[10] W. L. McMillan, Landau theory of charge density waves in transition-metal dichalcogenides, Phys. Rev. B **12**, 1187 (1975).

[11] O. Zachar, S. A. Kivelson, and V. J. Emery, Landau theory of stripe phases in cuprates and nickelates, Phys. Rev. B. **57**, 1422 (1998).

[12] L. Nie, A. V. Maharaj, E. Fradkin, and S. A. Kivelson, Vestigial nematicity from spin and/or charge order in the cuprates, Phys. Rev. B **96**, 085142 (2017).

[13] Y. Imry and S. K. Ma, Random-field instability of the ordered state of continuous symmetry, Phys. Rev. Lett. **35**, 1399 (1975).

[14] H. S. Kogon and D. J. Wallace, The Ising model in a random field; supersymmetric surface fluctuations and their implications in three dimensions, Journal of Physics A: Mathematical and General **14**, L527 (1981).

[15] E. Pytte, Y. Imry, and D. Mukamel, Lower critical dimension and the roughening transition of the random-field Ising model, Phys. Rev. Lett. **46**, 1173 (1981).

[16] M. Hagen, R. A. Cowley, S. K. Satija, H. Yoshizawa, G. Shirane, R. J. Birgeneau, and H. J. Guggenheim, Random fields and three-dimensional Ising models: $Co_xZn_{1-x}F_2$, Phys. Rev. B **28**, 2602 (1983).

[17] L. Nie, G. Tarjus, and S. A. Kivelson, Quenched disorder and vestigial nematicity in the pseudogap regime of the cuprates, Proc. Natl. Acad. Sci. U.S.A. **111**, 7980 (2014).